J|A|C|S
ARTICLES
Published on Web 06/12/2004

Bistabilities in 1,3,2-Dithiazolyl Radicals

Jaclyn L. Brusso,[1a] Owen P. Clements,[1a] Robert C. Haddon,[1b] Mikhail E. Itkis,[1b] Alicea A. Leitch,[1a] Richard T. Oakley,*[,1a] Robert W. Reed,[1a] and John F. Richardson[1c]

Contribution from the Department of Chemistry, University of Waterloo, Waterloo, Ontario N2L 3G1, Canada, Department of Chemistry and Center for Nanoscale Science and Engineering, University of California, Riverside, California 92521-0403, and Department of Chemistry, University of Louisville, Louisville, Kentucky 40292

Received March 10, 2004; E-mail: oakley@sciborg.uwaterloo.ca

Abstract: New synthetic methods for heterocyclic 1,3,2-dithiazolyl (DTA) radicals have been developed, and trends in the molecular spin distributions and electrochemical properties of a series of DTA radicals are reported. The crystal structures of [1,2,5]thiadiazolo[3,4-*f*][1,3,2]benzodithiazol-2-yl (TBDTA) and [1,3,2]-pyrazinodithiazol-2-yl (PDTA) have been determined. The structure of TBDTA (at 293 and 95 K) contains two molecules in the asymmetric unit, each of which generates π-stacked arrays, one consisting of antiparallel chains of centrosymmetrically associated dimers, the other comprising parallel chains of unassociated radicals. The structure of PDTA (at 293 and 95 K) is simpler, consisting of slipped stacks of π-dimers. Variable-temperature magnetic susceptibility (χ_P) measurements on TBDTA indicate essentially paramagnetic behavior for the unassociated radical π-stacks over the range 5−400 K. By contrast PDTA is diamagnetic at all temperatures below 300 K, but between 300 and 350 K the value of χ_P follows a sharp and well-defined hysteresis loop, with $T_C\downarrow = 297$ K and $T_C\uparrow = 343$ K. These features are symptomatic of a regime of bistability involving the observed low temperature π-dimer structure and a putative high-temperature radical π-stack. A mechanism for the interconversion of the two phases of PDTA and related structures is proposed in which hysteretic behavior arises from cooperative effects associated with the breaking and making of a lattice-wide network of intermolecular S- - -N′ and/or S- - -S′ interactions.

Introduction

The potential applications of organic radicals in molecular spin-electronic or "spintronic" devices has catalyzed efforts to develop new stable and magnetically active molecules.[2] Within this context the solid-state structures and magnetic properties of 1,3,2-dithiazolyl (DTA) radicals (Chart 1) have been a focus of recent research. However, despite the near-zero dimerization enthalpy of the dithiazolyl core,[3] the monocyclic derivatives **1** ($R_1 = R_2 =$ CN,[4] CF_3[5]) crystallize as diamagnetic dimers (at room temperature) aligned cofacially and linked by weak interannular S- - -S bonds; the dimers are then closely associated (pairwise) into tetrameric clusters. In condensed-ring dithiazolyls clustering of radicals is not observed, but spin-quenching is still possible, as in the benzene-based derivative BDTA **2**,[3] which displays a rare centrosymmetric mode of association. By contrast, the naphthalene compound NDTA **3** is paramagnetic (at room temperature). Its structure consists of discrete radicals locked into herringbone arrays,[6] with neighboring rings oriented in the "tilted-T" arrangement which favors structure-making CH- - -aromatic ring interactions.[7,8] Replacement of CH groups

Chart 1

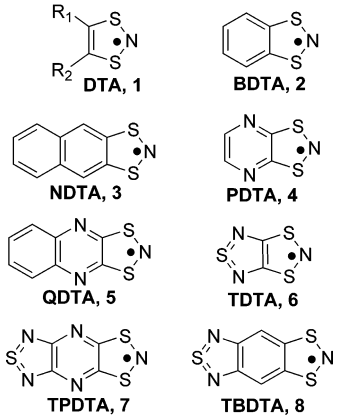

(1) (a) University of Waterloo. (b) University of California. (c) University of Louisville.
(2) (a) Miller, J. S.; Drillon, M. *Magnetism: Molecules to Materials II, Molecule-Based Materials*; Wiley-VCH: New York, 2001. (b) Gregg, J.; Allen, W.; Viart, N.; Kirschman, R.; Sirisathitkul, C.; Schille, J. P.; Gester, M.; Thompson, S.; Sparks, P.; Da Costa, V.; Ounadjela, K.; Skvarla, M. *J. Magn. Magn. Mater*. **1997**, *175*, 1. (c) Coey, J. M. D. *J. Magn. Magn. Mater*. **1999**, *197*, 1.
(3) (a) Awere, E. G.; Burford, N.; Haddon, R. C.; Parsons, S. Passmore, J. Waszczak, J. V.; White, P. S. *Inorg. Chem.* **1990**, *29*, 4821. (b) Awere, E. G.; Burford, N.; Mailer, C.; Passmore, J.; Schriver, M. J.; White, P. S. Banister, A. J.; Oberhammer, H.; Sutcliffe, L. H. *J. Chem. Soc., Chem. Commun*. **1987**, 66.
(4) Wolmershäuser, G.; Kraft, G. *Chem. Ber.* **1990**, *123*, 881.
(5) Du, H.; Haddon, R. C.; Krossing, I.; Passmore, J.; Rawson, J. M.; Schriver, M. J. *Chem. Commun*. **2002**, 1836.
(6) Barclay, T. M.; Cordes, A. W.; George, N. A.; Haddon, R. C.; Oakley, R. T.; Palstra, T. T. M.; Patenaude, G. W.; Reed, R. W.; Richardson, J. F.; Zhang, J. *J. Chem. Soc., Chem. Commun*. **1997**, 873.
(7) Hobza, P.; Selzle, H. L.; and Schlag, E. W. *J. Am. Chem. Soc*. **1994**, *116*, 3500

10.1021/ja048618m CCC: $27.50

by nitrogen, as in the pyrazine[9] and quinoxaline[6] derivatives PDTA **4** and QDTA **5**, militates against the "tilted-T" motif, and both these radicals adopt π-stacked structures. In PDTA the radicals were reported to be associated at room temperature, while in QDTA they remain undimerized, although on cooling the unpaired spins are quenched, presumably as a result of dimerization.[9]

In the thiadiazole- and thiadiazolopyrazine-based compounds, TDTA **6**[10,11] and TPDTA **7**,[12] there are no peripheral hydrogens, and consistently, slipped π-stack arrays are observed in the solid state. As an added feature both materials exhibit a form of bistability[13] in which a paramagnetic phase (undimerized π-stacks) coexists over a specific temperature range with a diamagnetic phase (π-dimer stacks).[14] The structural interconversions are characterized by a wide hysteresis loop in the temperature dependence of the magnetic susceptibility.

As a continuation of our magneto-structural investigations of condensed-ring 1,3,2-dithiazolyls, we have prepared and characterized the thiadiazolobenzene derivative TBDTA **8**, in which the pyrazine residue of TPDTA **7** has been replaced by a benzene ring. Our initial belief was that this minor molecular modification would not alter the slipped stack packing found for TPDTA and would allow a comparison of the degree of magneto-thermal hysteresis in the two compounds. We have also reexamined the pyrazine derivative PDTA **4**, in the hope of identifying a bistability similar to that found in TDTA **6**. Contrary to expectation, TBDTA adopts a crystal structure with subtleties hitherto unobserved for 1,3,2-DTA radicals and displays no magneto-thermal hysteresis. Satisfyingly, however, the magnetic susceptibility of PDTA exhibits a well-defined high-temperature hysteresis heralding the coexistence of two polymorphs. A mechanism for the phase interconversion of TDTA and PDTA is proposed to account for the bistability in these systems.

Results

Synthesis. Preparation of the initial target TBDTA **8** (Scheme 1) began with the oxidative thiocyanation of *o*-phenylenediamine **9** with bromine and potassium thiocyanate in methanol at −78 °C, to afford the bis-thiocyanate **10**. Although this reaction was reported over forty years ago,[15] a number of modifications, e.g., the use of low temperatures, slow addition rates, pH control during workup, were required to achieve consistent results. Closure of the thiadiazole ring with thionyl chloride, and reductive cleavage of the thiocyanate **11** with aqueous sulfide to yield the dithiol **12**, followed well-established procedures. Likewise oxidation of **12** to the bis(sulfenyl chloride) **13**, and cyclization of **13** with trimethylsilyl azide to the dithiazolylium

Scheme 1

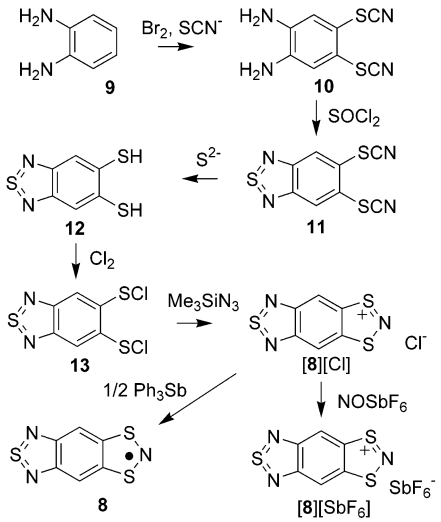

Scheme 2

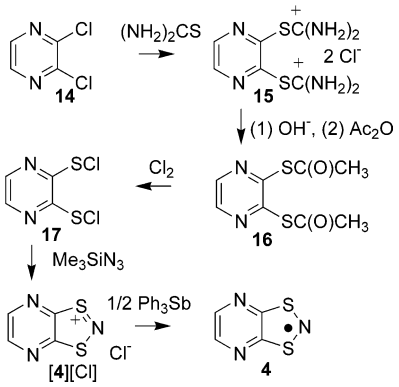

chloride [**8**][Cl], were quite straightforward. The latter compound could be metathesized to a hexafluoroantimonate salt [**8**][SbF_6] for characterization purposes or reduced directly with triphenylantimony to the desired radical TBDTA **8**. This latter step gave poor yields (<15%) regardless of the choice of solvent (acetonitrile or liquid SO_2), reductant (Ag, Zn, Ph_3Sb), or starting salt (chloride or hexafluoroantimonate). Once isolated, however, TBDTA was relatively air stable in the solid state and was easily purified by vacuum sublimation.

The pyrazine radical PDTA **4** was synthesized using a modification (Scheme 2) of the procedure originally described by Kraft and Wolmershäuser.[16] Accordingly, the dithiouronium salt **15**, prepared from dichloropyrazine **14**, was hydrolyzed in basic solution and the resulting dithiolate quenched with acetic anhydride (rather than acetic acid) to afford the bis-thioacetate **16**. After purification, the latter was converted into the bis(sulfenyl chloride) **17**, which was condensed with trimethylsilyl azide to give the crude dithiazolylium chloride salt [**4**][Cl]. As above, PDTA **4** was liberated by reduction of the crude salt with triphenylantimony and purified by vacuum sublimation.

EPR Spectra and Electrochemistry We have characterized the spin distribution of TBDTA **8** in solution by EPR spectroscopy. To place the results in context we have revisited the EPR spectra of compounds **2**−**7**. While hyperfine coupling constants have been reported for all of these materials,[3,12,17] the data refer

(8) (a) Gavezzotti, A.; Desiraju, G. R. *Acta Crystallogr.* **1988**, *B44*, 427. (b) Bernstein, J.; Sarma, J. A. R. P.; Gavezzotti, A. *Chem. Phys. Lett.* **1990**, *174*, 361.
(9) Heckman, G.; Johann, R.; Kraft, G.; Wolmershäuser, G. *Synth. Met.* **1991**, *41*−*43*, 3287.
(10) Fujita, W.; Awaga, K. *Science* **1999**, *286*, 261.
(11) McManus, G. D.; Rawson, J. M.; Feeder, N.; van Duijn, J.; McInnes, E. J. L.; Novoa, J. J.; Burriel, R.; Palacio, F.; Oliete, P. *J. Mater. Chem.* **2001**, *11*, 1992.
(12) Barclay, T. M.; Cordes, A. W.; George, N. A.; Haddon, R. C.; Itkis, M. E.; Mashuta, M. S.; Oakley, R. T.; Patenaude, G. W.; Reed, R. W.; Richardson, J. F.; Zhang, H. *J. Am. Chem. Soc.* **1998**, *120*, 352.
(13) (a) Kahn, O.; Martinez, C. J. *Science* **1998**, *279*, 44. (b) Kahn, O. *Chem. Br.* **1999**, *35*, 24.
(14) Itkis, M. E.; Chi, X.; Cordes, A. W.; Haddon, R. C. *Science* **2002**, *296*, 1443.
(15) Raby, C. *Ann. Chim.* **1961**, *6*, 481.
(16) Wolmershäuser, G.; Kraft, G. *Chem. Ber.* **1989**, *122*, 385.

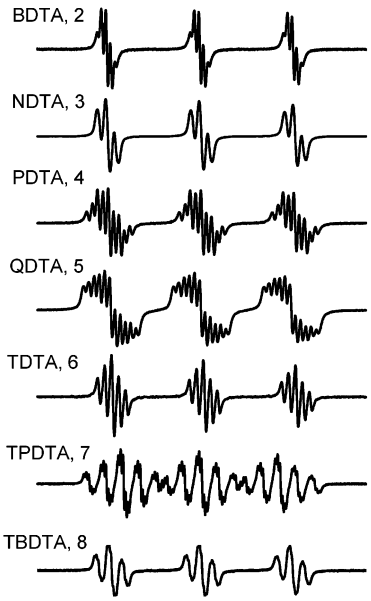

Figure 1. X-band EPR spectra of 1,3,2-DTA radicals, at 293 K in CH_2Cl_2, SW = 4.0 mT.

Table 1. Isotropic Hyperfine *g*-Values, Coupling Constants,[a] and Half-Wave[b] Potentials

radical	*g*	a_N	a_H	$E_2^{(-1/0)}$	$E_2^{(0/+1)}$
BDTA, **2**	2.0069	1.127	0.057, 0.045	−1.20[c]	0.15
		(1.130)	(−0.066, −0.047)		
NDTA, **3**	2.0067	1.140	0.097	−1.08[c]	0.27
		(1.128)	(−0.110)		
PDTA, **4**	2.0071	1.126, 0.070	0.120	−0.88[c]	0.53
		(1.118, 0.060)	(−0.104)		
QDTA, **5**	2.0065	1.089, 0.129	0.065, 0.023	−0.73[c]	0.62
		(1.099, 0.101)	(−0.050, −0.024)		
TDTA, **6**	2.0061	1.115, 0.084	−0.66[c]	0.65	
		(1.111, 0.082)			
TPDTA, **7**	2.0072	0.959, 0.209, 0.028		−0.06	1.06
		(1.032, 0.164, 0.038)			
TBDTA, **8**	2.0072	1.098, 0.020	0.16	−0.76	0.46
		(1.025, 0.036)	(−0.176)		

[a] In mT, X-band spectra at 293 K, in CH_2Cl_2; computed (B3LYP/6-31G**) values are in parentheses. [b] Volts vs SCE, in MeCN. [c] Irreversible wave, E_{pc} cited.

to the use of different temperatures, solvents, and even isotope content, and these variations hinder direct comparisons within the series. In addition we have in several cases been able to resolve several previously unresolved couplings. As may be seen in Figure 1, all the spectra (in CH_2Cl_2, 293 K) are characterized by a three-line pattern arising from strong hyperfine coupling to the dithiazolyl nitrogen. Delocalization of spin density from the DTA ring onto the adjacent ring leads to a slight decrease in value of a_N, and hyperfine coupling to the peripheral benzene protons, or pyrazine/dithiazole nitrogens, is observed. Additional but smaller coupling to the protons (or nitrogens) of the third ring can also be extracted by spectral simulation. Full analyses of the experimental spectra along with calculated (B3LYP/6-31G**) coupling constants are presented in Table 1. As noted elsewhere, the predictive ability of this level of theory is good.[18]

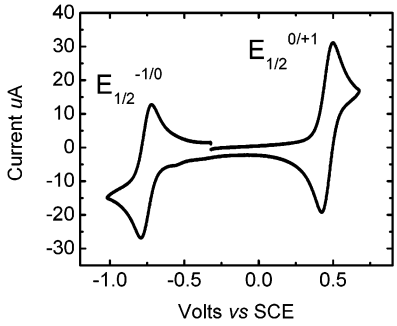

Figure 2. CV scan (100 mV/S) on TBDTA **8** in MeCN, [*n*-Bu_4N][PF_6] supporting electrolyte.

As might be expected, the spin distributions of TPDTA and TBDTA are similar, although the pyrazine residue in the former is a substantially more effective electron sink than a benzene ring.

To generate a quantitative comparison[19] of the redox properties of the heterocyclic 1,3,2-DTAs **2**−**8**, we have performed cyclic voltammetry measurements on the entire set. As an example the CV scan from −1.0 to +1.0 V (vs SCE) for TBDTA **8** is shown in Figure 2. The resulting half-wave potentials for oxidation and reduction for all the compounds are listed in Table 1. As can be seen from these data, variations in the nature of heterocyclic substituent have a major effect on the redox characteristics of the radical, e.g., the value of $E_{1/2}^{(0/+1)}$ changes by almost 1 V. All the radicals show a reversible wave for 0/+1 couple, but only for TPDTA and TBDTA are the waves for the −1/0 couple reversible. The new radical TBDTA can be considered a hybrid of several of the previously reported materials, but electrochemically the nearest match is with PDTA. From a chemical perspective, the relative ease of aerial oxidation of TBDTA, compared to the complete stability of TDTA and TPDTA toward molecular oxygen, is easily rationalized.

Crystal Structure of TBDTA 8. Blocklike crystals of TBDTA, grown by dynamic vacuum sublimation at 10^{-3} Torr along a temperature gradient of 100−45 °C, belong to the monoclinic space group $P2_1/c$. Single-crystal X-ray data obtained at 293 and 95 K are summarized in Table 2, and listings of pertinent intra- and intermolecular contacts are provided in Table 3. The most notable feature of this structure, which sets it apart from all other reported dithiazolyl radicals, is the presence of two environmentally distinct molecules (**A** and **B**) in the asymmetric unit, i.e., $Z = 8$. ORTEP drawings of the two molecules are shown in Figure 3. One of these (**A**) constitutes half of a centrosymmetric dimer, with an intradimer S1- - -S2′ distance of 3.252(2) Å at 293 K, while the other (**B**) remains unassociated. The S−N and S−C distances (Table 3) within the DTA rings of the two molecules are, however, remarkably similar, as expected from the fact that the enthalpy of dimerization of DTA radicals is negligible.[3] Other than a general shortening of both the unit cell parameters and the intermolecular distances, there is very little structural difference between the low- and high-temperature data.

The **A** and **B** molecules pack in slipped π-stack arrangements running along the *x*- and *z*-directions respectively, as illustrated in Figure 4. When the full unit cell is viewed along *z* (Figure 5), the ribbonlike nature of the molecular arrays becomes

(17) (a) Preston, K. F.; Sandall, J. P. B.; Sutcliffe, L. H. *Magn. Reson. Chem.* **1988**, *26*, 755. (b) Chung, Y.-L.; Sandall, J. P. B.; Sutcliffe, L. H.; Joly, H.; Preston, K. F.; Johann, R.; Wolmershäuser, G. *Magn. Res. Chem.* **1991**, *31*, 625. (c) Chung, Y.-L.; Fairhurst, S. A.; Gullies, D. G.; Kraft, G.; Krebber, A. M. L.; Preston, K. F.; Sutcliffe, L. H.; Wolmershäuser, G. *Magn. Reson. Chem.* **1992**, *30*, 774.
(18) Kaszynski, P. *J. Phys. Chem. A* **2001**, *105*, 7615.
(19) (a) Kaszynski, P. *J. Phys. Chem. A* **2001**, *105*, 7626. (b) Boeré, R. T.; Roemmele, T. L. *Coord. Chem. Rev.* **2000**, *210*, 369.

Table 2. Crystallographic Data

compound	TBDTA, **8**		LT-PDTA, **4**	
formula	$C_6H_2N_3S_3$	$C_6H_2N_3S_3$	$C_4H_2N_3S_2$	$C_4H_2N_3S_2$
fw	212.29	212.29	156.21	156.21
a, Å	9.938(3)	9.8847(6)	6.9963(7)	6.8564(8)
b, Å	22.373(6)	22.153(1)	7.8859(7)	7.8466(9)
c, Å	7.411(2)	7.2905(5)	11.4386(11)	11.3107(13)
α, deg	–	–	110.257(1)	109.965(2)
β, deg	111.761(4)	111.549(1)	95.155(2)	94.944(2)
γ, deg	–	–	103.625(2)	103.483(2)
V, Å^3	1530.5(7)	1484.8(2)	565.14(9)	546.95(11)
ρ(calcd), g cm^{-3}	1.843	1.899	1.836	1.897
space group	$P2_1/c$	$P2_1/c$	$P\bar{1}$	$P\bar{1}$
Z	8	8	4	4
temp, K	293(2)	95(2)	293(2)	95(2)
μ, mm^{-1}	0.902	0.929	0.828	0.856
λ, Å	0.71073	0.71073	0.71073	0.71073
data/restraints/parameters	2851/0/233	3121/0/233	2100/0/179	1965/ 0/179
solution method	direct methods	direct methods	direct methods	direct methods
R, R_w (on F^2)[a]	0.0423, 0.0915	0.0303, 0.0691	0.0341, 0.0879	0.0339, 0.0801

[a] $R = [\sum||F_o| - |F_c||]/[\sum|F_o|]$ for $I > 2\sigma(I)$; $R_w = \{[\sum w|F_o|^2 - |F_c|^2|^2]/[\sum(w|F_o|^4)]\}^2$.

Table 3. Summary of Intra- and Intermolecular Distances (Å)[a] in TBDTA **8**

	molecule **A**			molecule **B**	
	293 K	95 K		293 K	95 K
S1−N1	1.640(2)	1.644(2)	S4−N4	1.647(2)	1.652(2)
S2−N1	1.648(2)	1.648(2)	S5−N4	1.645(2)	1.648(2)
S1−C1	1.749(2)	1.749(2)	S4−C7	1.746(2)	1.747(2)
S2−C2	1.750(2)	1.746(2)	S5−C8	1.744(2)	1.748(2)
S1- - -S2′	3.252(2)	3.201(2)[b]	–		
S3- - -S2′	3.579(2)	3.514(2)[c]	S6- - -S4′	3.565(2)	3.501(2)[c]
S3- - -N1′	3.243(2)	3.174(2)[c]	S6- - -N4′	3.190(2)	3.109(2)[c]

[a] ESDs are in parentheses. [b] Intradimer contacts. [c] Lateral contacts.

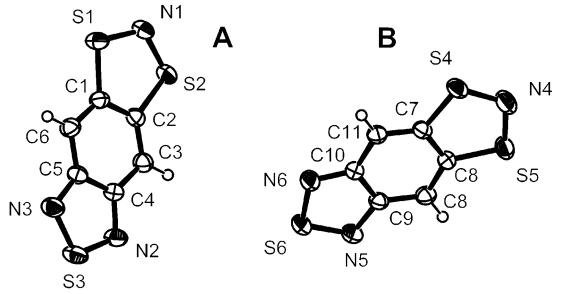

Figure 3. ORTEP drawing (50% probability ellipsoids) of the asymmetric unit of TBDTA **8** (at 293 K), showing atom numbering.

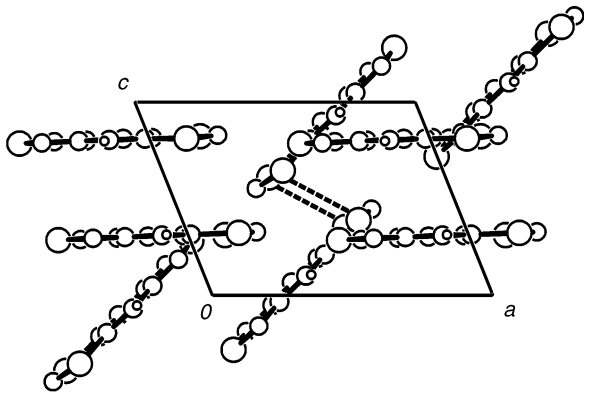

Figure 4. Packing of TBDTA **8**, viewed down *y*, showing the crossed *π*-stack arrays. The dashed lines connect the sulfurs of the centrosymmetric dimers of radical **A**.

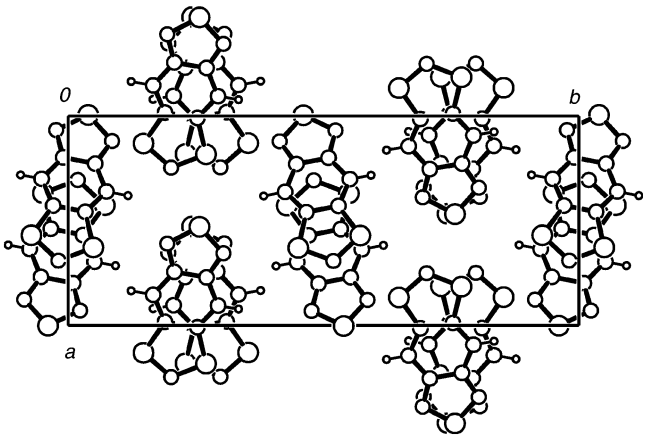

Figure 5. Unit cell of TBDTA **8**, viewed down *z*, showing ribbons of **A** (at $y = 0$, 1/2, 1) and **B** (at $y = 1/4$, 3/4).

evident. Within the **B** stacks consecutive molecules along *z* are slightly offset to either side of the glide plane (at $y = 1/4$, 3/4), while in the **A** stacks neighboring molecules are related by centers of symmetry. In both stacks neighboring molecules along the ribbons are connected by close (shorter than van der Waals[20]) S- - -N′ and S- - -S′ contacts (Table 3). A comparison of the layers within the two *π*-stacks (Figure 6) illustrates the antiparallel nature of neighboring **A** stack ribbons, which sets up the centrosymmetric dimerization mode noted above. By contrast, all the molecules within the **B** stacks run parallel.

Crystal Structure of LT-PDTA. PDTA **4** can exist in one of two polymorphs, hereafter referred to as the low-temperature (LT) and high-temperature (HT) phases.[21] In this contribution we describe the crystal structure of the former. Lustrous blue-black rods of LT-PDTA suitable for X-ray work were grown by static (sealed tube) sublimation at 10^{-2} Torr along a temperature gradient of 60−30 °C. Under these conditions it is likely that both polymorphs, i.e., the LT and HT phases, are produced, but upon slow cooling of the sublimate to room temperature the HT phase slowly reverts to the LT form. Close inspection of the harvested sublimate revealed that the majority of crystals were heavily twinned. This observation may reflect the fact that the HT phase is itself twinned or that twinning is

(20) Bondi, A. *J. Phys. Chem.* **1964**, *68*, 441
(21) The packing pattern of LT-PDTA was communicated some years ago by Wolmershäuser and co-workers (ref 9), but details of the crystal data and structural parameters were not reported.

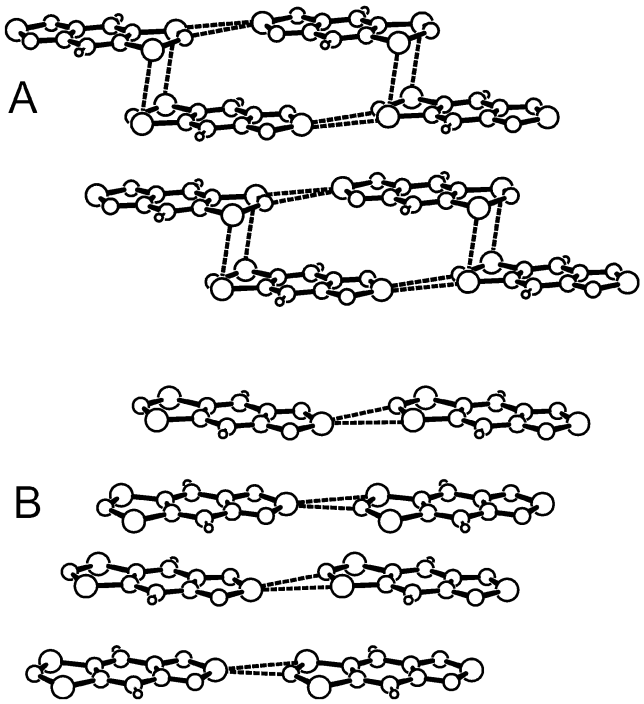

Figure 6. Slipped π-stacks of **A** and **B** molecules in TBDTA **8**. Intermolecular S- - -S′ and S- - -N′ contacts (dashed lines) are defined in Table 3.

Table 4. Summary of Intra- and Intermolecular Distances (Å)[a] in LT-PDTA **4**

	293 K	95 K		293 K	95 K
S1−N2	1.645(2)	1.647(2)	S1−C1	1.737(2)	1.743(2)
S2−N2	1.648(2)	1.657(2)	S2−C2	1.743(2)	1.747(2)
S3−N5	1.647(2)	1.651(2)	S3−C6	1.736(2)	1.737(2)
S4−N5	1.650(2)	1.654(2)	S4−C5	1.741(2)	1.743(2)
S1- - -S3′	3.322(2)	3.257(2)[b]	S2- - -S4′	3.272(2)	3.212(2)[b]
S1- - -S3′	3.826(2)	3.768(2)[c]	S2- - -S4′	3.874(2)	3.812(2)[c]
S1- - -S1′	3.407(2)	3.294(2)[d]	S1- - -S3′	3.343(2)	3.268(2)[d]
S2- - -N4′	2.914(2)	2.841(2)[d]	S4- - -N3′	2.929(2)	2.875(2)[d]

[a] ESDs are in parentheses. [b] Intradimer contacts. [c] Interdimer contacts along stack. [d] Lateral contacts between stacks.

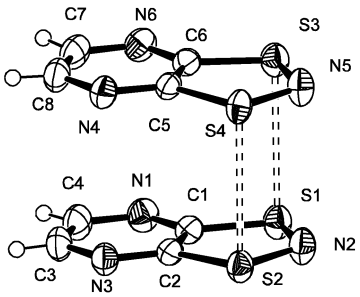

Figure 7. ORTEP drawing (50% probability ellipsoids) of the LT-PDTA dimer, showing atom numbering.

introduced in the phase reversion. Either way, careful screening eventually afforded a few untwinned crystals of the LT phase. Single-crystal X-ray data on this phase, obtained both at 293 and 95 K, are summarized in Table 2, and listings of pertinent intra- and intermolecular contacts are provided in Table 4.

Crystals of LT-PDTA belong to the triclinic space group $P\bar{1}$ and consist of centrosymmetric pairs of PDTA dimers; an ORTEP drawing is shown in Figure 7. The intramolecular S−N and S−C distances within both halves of the dimer are

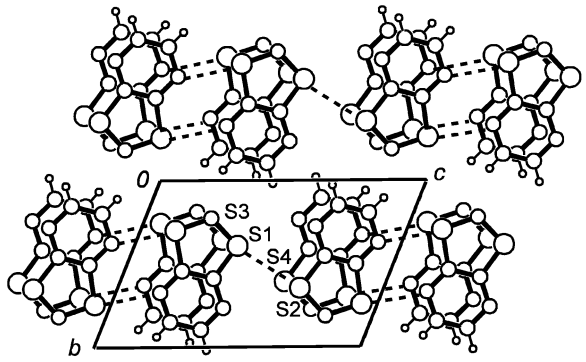

Figure 8. Unit cell of LT-PDTA. Lateral S- - -S′ and 6-center S- - -N′ contacts (dashed lines) are defined in Table 4.

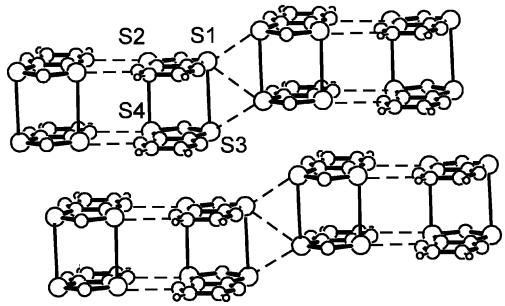

Figure 9. Slipped π-stacks of LT-PDTA dimers. Intermolecular S- - -S′ and S- - -N′ contacts (dashed lines) are defined in Table 4.

unremarkable, mirroring those seen in TBDTA and other DTA radicals, and while there is a general shortening of intramolecular bond lengths occasioned by cooling, there is very little structural difference between the 293 and 95 K data. The intermolecular distances, notably the intradimer S- - -S′ contacts (3.322(2) and 3.272(2) Å), are more interesting. These are longer than those observed in the centrosymmetric dimers of TBDTA and BDTA, resembling more nearly those seen in the cofacial dimers of the LT phases of TDTA and TPDTA. On cooling from 293 to 95 K, these dimer S- - -S′ interactions are also subject to a much larger contraction (to 3.257(2) and 3.212(2) Å) than the intramolecular bonds. The lateral S- - -S′ interactions S1- - -S3′ and S1- - -S1′ are also subject to a large contraction on cooling.

Dimers of LT-PDTA form ribbonlike arrays of centrosymmetrically locked pairs running along the *z*-direction. As the unit cell drawing in Figure 8 illustrates, there are several close lateral intermolecular S- - -S′ (S1- - -S1′ and S1- - -S3′) and S- - -N′ (S2- - -N4′ and S4- - -N3′) contacts within and between these pairs of dimers. Indeed, the efficiency with which neighboring molecules couple across inversion centers is a critical feature of this structure. Similar packing arrangements, with 6-center S- - -N′ bridges, are observed in TDTA and TPDTA, and as discussed below, the bistability found in all these compounds can be related to the role these interactions play. This kind of nesting is, of course, precluded in TBDTA by the presence of the buffering CH units.

Figure 9 illustrates the slipped π-dimer stacks, viewed from a direction approximately parallel to the ribbonlike molecular arrays. The offset of the dimers along the stack, characterized by the interdimer S- - -S′ interactions S1- - -S3′ and S2- - -S4′, is clearly apparent, as are the lateral S- - -S′ and S- - -N′ contacts noted above. The ramifications of these features on the magnetic properties of the material are described below.

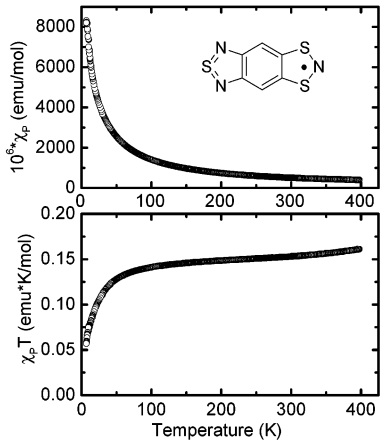

Figure 10. Plots of χ_P and $\chi_P T$ as a function of T for TBDTA **8**.

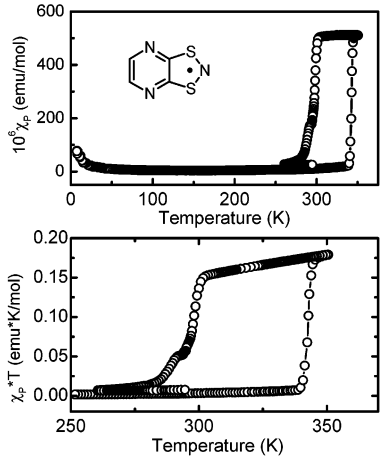

Figure 11. Plots of χ_P and $\chi_P T$ as a function of T for PDTA **4**.

Magnetic Measurements. Variable-temperature magnetic susceptibility (χ) measurements have been performed on microcrystalline samples of both TBDTA **8** and PDTA **4**. The results, expressed in the form of plots of χ_P vs T and $\chi_P T$ vs T, where $\chi_P = \chi + \chi_0$ and χ_0 is the calculated diamagnetic correction based on Pascal's constants, are presented in Figures 10 and 11.

Taking into account that 50% of the $S = 1/2$ radical centers in TBDTA exist in the form of presumably diamagnetic dimers, the temperature dependence of the susceptibility χ_P over the range 4−400 K is well described within a Curie−Weiss framework, with $C = 0.158$ and $\Theta = -12$ K. A plot of $\chi_P T$ vs T also shows the expected features, i.e., a relatively invariant regime from 50 to 350 K with a value near 0.15, a little less than half that expected if all the spins uncoupled. There is a slight increase in $\chi_P T$ above 350 K, perhaps indicative of some spin unpairing of the dimers, and there is also a weak antiferromagnetic tail below 50 K. Overall, however, the results reveal a remarkably rigid system, with little if any structural or magnetic variations over a wide temperature range. This, in itself, represents a unique finding in 1,3,2-DTA structures.

The magnetic behavior of PDTA is more dramatic. At and below room temperature the material is essentially diamagnetic, as expected from the dimeric association observed in the 293 and 95 K crystal structures. We ascribe the residual paramagnetism to the presence of lattice defects which, if expressed in terms of the molar fraction of Curie spins, amount to less than 0.15%. Upon heating above room temperature no change in χ_P is observed until near 340 K, whereupon a sudden increase takes place, reaching a plateau around 350 K which, expressed in terms of $\chi_P T$, corresponds to about one-half the value expected (0.375) if the radicals were dissociated completely into noninteracting $S = {}^1/_2$ paramagnets. Cooling the sample leads to little change in χ_P , but a slight and steady decrease in $\chi_P T$ until a temperature of 300 K is reached, whereupon a sharp decrease in χ_P and $\chi_P T$ takes place, returning both functions to near their initial room-temperature values. The resulting well-defined hysteresis loop for both χ_P and $\chi_P T$ is the magnetic signature of the kind of bistability noted earlier for TPDTA and TDTA, i.e., the coexistence of a diamagnetic π-stacked dimer (LT-PDTA) and a paramagnetic π-stacked radical (HT-PDTA). In the present case the regime of bistability ($T_C{\downarrow} = 297$ K and $T_C{\uparrow} = 343$ K) for the two phases spans higher temperatures than those observed for TDTA[10,11] ($T_C{\downarrow} = 234$ K and $T_C{\uparrow} = 316$ K) and TPDTA[12] ($T_C{\downarrow} = 120$ K and $T_C{\uparrow} = 180$ K).

The failure of $\chi_P T$ to reach the expected value of 0.375 for an $S = {}^1/_2$ system value, coupled with the steady decrease in $\chi_P T$ upon cooling over the range 350−300 K, likely heralds the presence of antiferromagnetic coupling both along and between the radical π-stacks in the HT phase; similar features were earlier noted for TDTA.[10,11]

Discussion

The existence of polymorphism in sulfur nitrogen radicals is well documented,[22,23] but bistability, involving the hysteretic interconversion of two structurally and energetically similar polymorphs, is rare. The earliest indication of the phenomenon was noted over a decade ago in the biradical[24] 1,3-phenylene-bis(dithiadiazolyl),[25] a diamagnetic stacked π-dimer structure which dissociated at elevated temperatures with a concomitant increase in χ. Upon cooling the sample some paramagnetism was retained, but the efficiency of the cycling process was poor. The hysteretic bistability observed later in the two 1,3,2-DTA radicals TPDTA[12] and TDTA[10,11] provided more dramatic and elegant manifestations, particularly in the case of TDTA, of the coexistence over a wide temperature range of two distinct but related structures, one diamagnetic, the other paramagnetic. The driving force for change from the HT phase to LT phase is a charge density wave (CDW) driven or Peierls instability,[26] a pervasive feature of many sulfur nitrogen radicals. In the case of TPDTA the mechanism of the phase interconversion has been

(22) (a) Cordes, A. W.; Haddon, R. C.; Hicks, R. G.; Oakley, R. T.; Palstra, T. T. M. *Inorg. Chem.* **1992**, *31*, 1802. (b) Bryan, C. D.; Cordes, A. W.; Haddon, R. C.; Hicks, R. G.; Kennepohl, D. K.; MacKinnon, C. D.; Oakley, R. T.; Palstra, T. T. M.; Perel, A. S.; Scott, S. R.; Schneemeyer, L. F.; Waszczak, J. V. *J. Am. Chem. Soc.* **1994**, *116*, 1205.

(23) (a) Banister, A. J.; Bicklebank, N.; Clegg, W.; Elsegood, M. R. J.; Gregory, C. I.; Lavender, I.; Rawson, J. M.; Tanner, B. K. *J. Chem. Soc., Chem. Commun.* **1996**, 679. (b) Banister, A. J.; Bicklebank, N.; Lavender, I.; Rawson, J. M.; Tanner, B. K, Clegg, W.; Elsegood, M. R. J.; Palacio, F. *Angew. Chem., Int. Ed. Engl.* **1996**, *35*, 2533. (c) Palacio, F.; Antorrena, G.; Castro, M.; Burriel, R.; Rawson, J. M.; Smith, J. N. B.; Bricklebank, N.; Novoa, J.; Ritter, C. *Phys. Rev. Lett.* **1997**, *79*, 2336. (d) Bond, A. D.; Haynes, D. A.; Pask, C. M.; Rawson, J. M. *J. Chem. Soc., Dalton Trans.* **2002**, 2522.

(24) Magnetic bistability has recently been observed in a nitroxide biradical. See: Shultz, D. A.; Fico, R.; Boyle. P. D.; Kampf, J. W. *J. Am. Chem. Soc.* **2001**, *123*, 10403.

(25) Andrews, M. P.; Cordes, A. W.; Douglass, D. C.; Fleming, R. M.; Glarum, S. H.; Haddon, R. C.; Marsh, P.; Oakley, R. T.; Palstra, T. T. M.; Schneemeyer, L. F.; Trucks, G. W.; Tycko, R. R.; Waszczak, J. V.; Warren, W. W.; Young, K. M.; Zimmerman, N. M. *J. Am. Chem. Soc.* **1991**, *113*, 3559.

(26) Peierls, R. C. *Quantum Theory of Solids*; Oxford University Press: London, 1955; p 108.

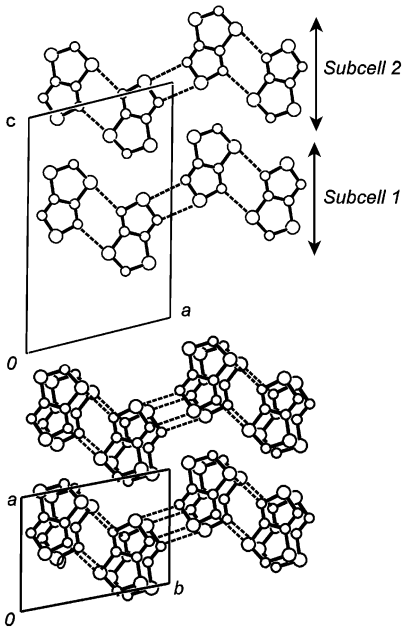

Figure 12. Crystal structures of HT-TDTA (above) and LT-TDTA (below). Intermolecular (4-center and 6-center) S- - -N′ contacts are shown with dashed lines.

described in terms of a tectonic plate slippage of layers within an eight-layer supercell common to both lattices.[12] Interestingly in the TBDTA structure reported here one of the two sublattices consists of a radical π-stack, but the presence of a dimer π-stack in the other sublattice, and a consequent cell doubling, precludes the possibility of a Peierls instability in the radical stack. This material thus represents the first example of a DTA radical stack in which dimerization is completely suppressed.

To date there has been no attempt to probe the mechanistic aspects of the bistability in TDTA,[10,11]and with the discovery of bistability in PDTA the need to address these issues becomes more acute. To this end we focus first on TDTA, where the structures of both the HT and LT phases have been established crystallographically. The crystal structures of both forms, viewed down the stacking axes, are shown in Figure 12.[27] While the space groups ($P2_1/c$ and $P\bar{1}$) are different, the overall appearance of the structures are remarkably similar. Both present ribbonlike arrays of TDTA running laterally across the cells, and linked by a series of intermolecular S- - -N′ interactions which span inversion centers to produce 4-center and 6-center bridges.[28] There are, however, notable differences. For example, along the stacking direction the unit cell dimension of the LT-phase is doubled, heralding the presence of dimers.

Of greater importance, in terms of the structural interconversion pathway, is the fact that the unit cell length $c = 15.0630(13)$ Å in the HT form is twice that of the corresponding dimension $a = 7.5310(5)$ Å in the LT form. As a result there are two ribbonlike arrays per cell, denoted subcells 1 and 2 in Figure 12; these ribbons are *not* coplanar. Whereas in the LT form the molecular ribbons all run parallel to [0,0,1], i.e., the *xy* plane, alternate ribbons along the *z*-direction in the HT phase are rotated clockwise and anticlockwise about the *z* axis. As a result the mean planes of the ribbons in subcell 1 are coplanar with the [1,−1,0] plane, while those in subcell 2 are coplanar with the [1,1,0] plane. These critical structural features are illustrated in Figure 13, which shows the stacking of ribbons in the two sub-cells of the HT form, and the ribbons of dimers found in the LT form. On the basis of the above structural description of LT- and HT-TDTA, it is clear that a simple tectonic plate interconversion mechanism, of the type seen in TPDTA,[12] does not apply; more subtle structural changes are required.

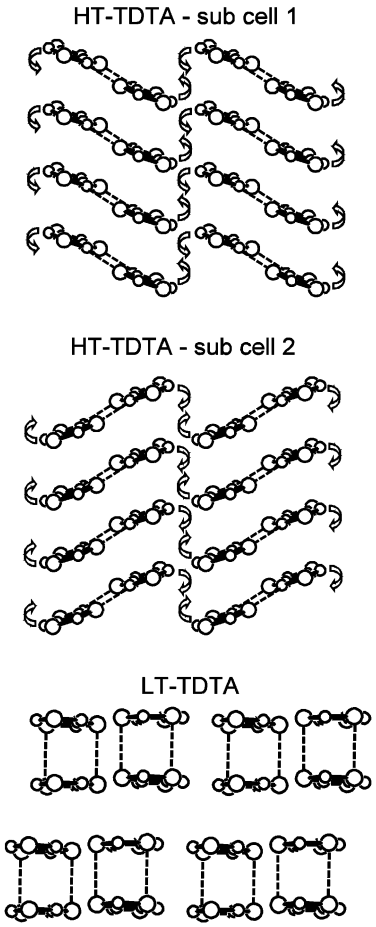

Figure 13. End-on views of subcells 1 and 2 of HT-TDTA (along *z*), and LT-TDTA (along *x*). Curved arrows denote motion required for phase interconversion.

To effect the necessary changes, we propose a "domino" mechanism to convert the molecular ribbons, tilted clockwise and anticlockwise in the two subcells of the HT form, into the horizontal ribbons found in the LT form. As a first step in this process, segmentation of the ribbons is required. This can occur at either of the two bridge bonds, i.e., the 4-center or 6-center linkages illustrated in Figure 12. On the basis of the shortness of the 6-center S- - -N′ bridges, we suggest that the 4-center S- - -N′ links are weaker and the more likely to open. Accordingly, if these bonds break, the ribbons are divided into pairs of TDTA molecules laterally bridged by the remaining 6-center S- - -N′ interactions. Once disconnected from their neighbors, these supermolecules (Figure 14) are free to rotate, clockwise or anticlockwise, about the center of symmetry on which they hinge so as to produce, eventually, the horizontal coplanar arrangement characteristic of the LT-modification. Lateral 4-center linkages can then reform, and dimerization takes place.

(27) The structural account on TDTA has been constructed using the crystallographic data reported in ref 10.
(28) In the LT- and HT-TDTA structures (both at 298 K, ref 10) the 4-center S- - -N bridges are 3.088(2) and 3.132(2) Å, respectively, while the 6-center S- - -N bridges are 2.959(2) and 3.018(2) Å, respectively.

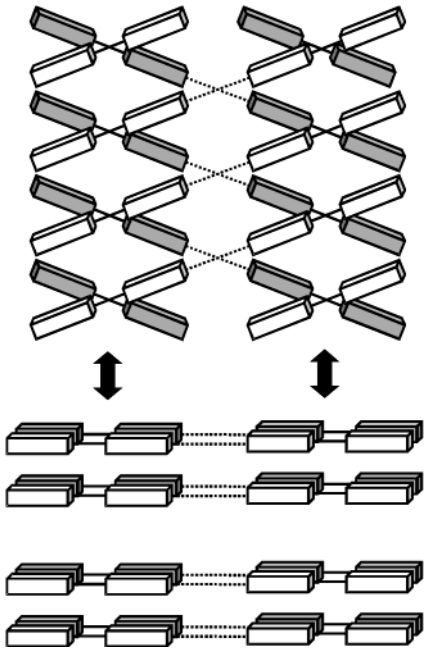

Figure 14. Domino interconversion of HT-TDTA (above) and LT-TDTA (below), with cleavage and reformation of 4-center S- - -N′ interactions (dashed lines).

Chart 2

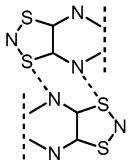

Minor tectonic plate slippage required to map exactly onto the final slipped π-dimer stack can also occur.

The domino mechanism described above relies on the presence and preservation of the inversion symmetry; the molecular plates rotate about the 6-center bridges, and all bond-making and -breaking processes occur at the 4-center bridges. It leads to a halving of the unit cell in one dimension and a doubling in another. It requires, as a rate-determining step in both the forward (dimerization) and backward (dissociation) directions, the rupture of the strong electrostatic S- - -N′ contacts which characterize both phases. Most appealing, however, is the way in which cooperativity emerges as natural consequence of the domino mechanism. Accordingly the rate of phase interconversion, once initiated, will accelerate as the new lattice self-assembles and new bridge bonds are built.

Detailed analysis of the phase interconversion mechanism of PDTA is precluded by the absence of structural information on the high-temperature phase. Nonetheless, comparison of the packing of the LT forms of PDTA and TDTA reveals many common features, notably the presence of centrosymmetric pairs (Chart 2) linked by 6-center S- - -N′ contacts (Figures 8 and 9), suggesting that similar structural issues are involved. However, in contrast to TDTA, there is a "weak link" in the ribbonlike arrays of PDTA molecules. This arises from the fact that PDTA cannot form centrosymmetric 4-center S- - -N′ bridges at all, as there is no thiadiazole ring. There are weak S- - -S′ interactions which serve to link the 6-center linked supermolecules, but these are likely to be cleaved more easily. Thus, even without any direct structural information on the HT phase of PDTA, it is reasonable to anticipate that the regime of bistability found for PDTA should be less than that found for TDTA, although considerably greater than that found in TPDTA, where cooperative effects associated with tectonic plate motion are less pronounced. Finally, in QDTA, the absence of hysteresis/cooperativity can be directly attributed to the space group $P2_1$, which precludes pairwise centrosymmetric intermolecular linkages. While there are lateral S- - -N′ contacts in QDTA, they are considerably longer (3.507(1) Å), and insufficient to generate any significant barrier, let alone apportion a cooperative effect, to the association/dissociation process.

Conclusions and Summary

In the course of searching for new molecular radical materials we have prepared and characterized the two 1,3,2-dithiazolyl radicals, TBDTA and PDTA, comparing along the way their spin distributions and electrochemical properties with those of other condensed-ring 1,3,2-dithiazolyls. From a structural perspective our intent was to design slipped π-stack structures exhibiting magnetic bistability. Attempts, however, to design molecular materials with specific crystal structures remains, at best, a sporting past-time,[29] and our efforts produced some unexpected results. In the case of TBDTA, a system closely related in terms of size, shape, and spin distribution to TDTA and TPDTA, two radicals known to form bistable π-stacks, a complex structure was found that consists of two very different sublattices, one based on a radical π-stack and the other on a π-dimer stack. Dimerization, let alone bistability, of the resulting open-shell sublattice is not possible. By contrast, the known radical PDTA, earlier described as a dimer π-stack, has been found to exhibit a wide and sharply defined magnetic hysteresis above room temperature.

To account for the dramatic hysteresis exhibited by both TDTA and PDTA, we have developed a mechanism for their phase interconversion, one which involves the cooperative breaking and making of strong intermolecular S- - -N′ interactions and a domino-like rotation of molecules within the π-stacked structure. The model allows the development of at least empirical guidelines for the pursuit of other bistable radical-based materials. Whether these radical/dimer bistabilities will find applications in switching devices[30] remains to be seen.

Experimental Section

General Procedures and Starting Materials. The reagents *o*-phenylenediamine **9**, potassium thiocyanate, bromine, thionyl chloride, pyridine, dichloropyrazine **14**, thiourea, acetic anhydride, sodium sulfide nonahydrate, nitrosonium hexafluoroantimonate, trimethylsilyl azide, and triphenylantimony (all from Aldrich) and chlorine gas (Matheson) were obtained commercially and used as received. Samples of radicals **2**,[3] **3**,[12] **5**,[12] **6**,and **7**[12] (for EPR and CV work) were all prepared according to literature procedures. All solvents were at least of reagent grade; acetonitrile (MeCN) and dichloroethane (DCE) were dried by distillation from P_2O_5. All reactions were performed under an atmosphere of dry nitrogen. Melting points are uncorrected. Fractional sublimations were performed in an ATS series 3210 three-zone tube furnace, mounted horizontally, and linked to a series 1400 temperature

(29) Enkelmann, V. *Angew. Chem., Int. Ed. Engl.* **1991**, *30*, 1121.
(30) Miller, J. *Angew. Chem., Int. Ed.* **2003**, *42*, 27.
(31) (a) Kraft, G. Dissertation, Universität Kaiserslautern, 1989. (b) Wolmershäuser, G.; Johann, R. *Angew. Chem., Int. Ed. Engl.* **1989**, *28*, 920.
(32) When crude **9** was used, yields were nearer 40−50%.

control system. Infrared spectra (Nujol mulls, KBr optics) were recorded on a Nicolet Avatar FTIR spectrometer (at 2 cm^{-1} resolution). ^1H NMR spectra were run on a Bruker Avance 300 MHz NMR spectrometer. Elemental analyses were performed by MHW Laboratories, Phoenix, AZ 85018.

Preparation of 1,2-Diamino-benzene-4,5-bis(thiocyanate) 10. A solution of bromine (29.8 g, 0.190 mol) in 100 mL of cold MeOH was added slowly over 2−3 h to a solution of potassium thiocyanate (36.1 g, 0.370 mol) and *o*-phenylenediamine **9** (10.0 g, 0.0930 mol) in 500 mL of MeOH at −78 °C. The mixture was allowed to warm slowly to room temperature and was poured into 1 L of water. The resulting dark-red slurry was filtered and the filtrate made basic by the addition of aqueous ammonia. The bright-yellow precipitate so formed was filtered off, washed with water, and air-dried. The crude product **10** (9.80 g, 0.044 mol, 48%) was purified by passing a solution of it in ethyl acetate through a bed of silica. Removal of the solvent from the eluate and recrystallization from chlorobenzene afforded pale-yellow feathers, dec >135 °C. IR: 3459 (w), 3423 (m), 3378 (m), 2163 (m), 1662 (m), 1615 (m), 1563 (s), 1496 (m), 1310 (m), 1230 (w), 861 (m), 676 (w) cm^{-1}. ^1H NMR (δ, DMSO) 6.90 (s, 2H), 5.47 (s, br, 4H). Anal. Calcd for $C_8H_6N_4S_2$: C, 43.22; H, 2.72; N, 25.20%. Found: C, 43.40; H, 2.68; N, 25.35%.

Preparation of 2,1,3-Benzenethiadiazole-5,6-bis(thiocyanate) 11. Thionyl chloride (3.90 g, 32.7 mmol) was added to the slurry of recrystallized 1,2-diaminobenzene-bis(thiocyanate) **10** (2.22 g, 10.0 mmol) in 75 mL of toluene. Three drops of pyridine were added, and the mixture was set to reflux under N_2 for 1 h. After cooling the resulting dark-brown solution to room temperature, 5 mL of ethanol was added to quench residual thionyl chloride. The mixture was filtered and the solvent removed from the filtrate to leave a yellow solid that was recrystallized from ethanol to give off-white flakes of **11** (1.94 g, 7.75 mmol, 78%),mp 115−117 °C. IR: 3063 (w), 2168 (m), 1357 (w), 1237 (m), 974 (m), 913 (w), 863 (m), 858 (s), 854 (s), 831 (s), 708 (w), 539 (s), 422 (s) cm^{-1}. ^1H NMR (δ, $CDCl_3$) 8.58 (s, 2H). Anal. Calcd for $C_8H_2N_4S_3$: C, 38.38; H, 0.81; N, 22.38%. Found: C, 38.21; H, 0.59; N, 22.44%.

Preparation of 2,1,3-Benzenethiadiazole-5,6-dithiol 12. Compound **11** (1.94 g, 7.75 mmol) was added as a solid to a solution of $Na_2S\cdot 9H_2O$ (6.0 g, 25.0 mmol) in 100 mL of degassed water and the mixture heated to ∼70 °C for 30 min to produce a clear, orange-red solution. The mixture was cooled to room temperature, and 20 mL of 10% HCl was added dropwise to afford a heavy, pale-yellow precipitate. The precipitate was filtered off, washed with water, and air-dried. The product **12** (1.51 g, 7.53 mmol, 97%) was purified by vacuum sublimation at 90 °C/10^{-2} Torr and recrystallized from hexane as canary-yellow needles, mp 135−136 °C. IR: 3057 (w), 2531 (w), 1436 (w), 1240 (m), 1093 (w), 998 (m), 857 (s), 710 (w), 529 (m), 489 (m) cm^{-1}. ^1H NMR (δ, $CDCl_3$) 8.03 (s, 2H), 3.98 (s, 2H). Anal. Calcd for $C_8H_4N_2S_3$: C, 35.98; H, 2.01; N, 13.99%. Found: C, 35.95; H, 1.82; N, 13.72%.

Preparation of 2,1,3-Benzenethiadiazole-bis(sulfenyl chloride) 13. Chlorine gas was passed over a solution of **12** (0.850 g, 4.25 mmol) in 10 mL of DCE held in an ice/water bath. A gelatinous, yellow solid (the disulfide) immediately precipitated and then redissolved after a few minutes to form a canary-yellow solution. The solvent and residual chlorine were flash distilled to leave **13** as a yellow solid. IR: 3088 (w), 1747 (w), 1653 (w), 1570 (m), 1487 (m), 1438 (m), 1417 (w), 1353 (w), 1233 (m), 1223 (w), 982 (m), 876 (s), 861 (s), 826 (s), 719 (m), 708 (w), 532 (s), 493 (s), 457 (s), 421 (s) cm^{-1}. This material was used in subsequent steps without further purification.

Preparation of [1,2,5]Thiadiazolo[3,4-*f*][1,3,2]benzodithiazolylium Chloride [8][Cl] and Hexafluoroantimonate [8][SbF_6]. The bis-(sulfenyl chloride) **13** obtained as described above was dissolved in 15 mL of DCE. To this stirred solution was added dropwise a solution of trimethylsilyl azide (0.488 g, 4.25 mmol) in 5 mL of DCE, producing a heavy, maroon precipitate. After 30 min the product [**8**][Cl] was filtered off, washed with 2 × 15 mL of DCE, and dried in vacuo; crude yield 0.96 g (0.38 mmol, 91%). IR: 3054 (w), 1421 (w), 1216 (w), 1043 (m), 880 (s), 824 (w), 770 (m), 535 (m), 429 (m) cm^{-1}. This material was metathesized with $NOSbF_6$ (1.24 g, 4.67 mmol mmol) in 25 mL of MeCN, to afford a dark-red solution. Filtration of the solution, and flash distillation of the solvent from the filtrate afforded a dark-red solid that was recrystallized from acetic acid as red/black crystals of [**8**][SbF_6] (0.98 g, 2.21 mmol, 52% based on **12**), dec >205 °C. IR: 3112 (w), 1419 (w), 1288 (w), 1169 (w), 1050 (m), 965 (m), 892 (m), 864 (m), 850 (w), 773 (s), 664 (vs), 647(vs), 558 (m), 535 (w), 430 (m) cm^{-1}. Anal. Calcd for $C_6H_2N_3S_3F_6Sb$: C, 16.08; H, 0.45; N, 9.38%. Found: C, 16.38; H, 0.53; N, 9.18%.

Preparation of [1,2,5]Thiadiazolo[3,4-*f*][1,3,2]benzodithiazol-2-yl TBDTA 8. Triphenylantimony (0.736 g, 2.06 mmol) was added to a cold (−20 °C) slurry of crude [**8**][Cl] (0.937 g, 3.82 mmol) in 20 mL of degassed MeCN, and the mixture was allowed to warm slowly to room temperature. After 30 min the red/black solid was filtered off, washed with 2 × 10 mL of MeCN, and dried in vacuo. The crude product **8** was purified by gradient tube sublimation over a range of 100−45 °C/10^{-3} Torr. Yields of sublimed material, dec >140 °C, were generally low, never surpassing 20% (based on crude [**8**][Cl]). IR: 3077 (w), 1438 (w), 1413 (w), 1236 (m), 1042 (w), 912 (w), 870 (m), 863 (s), 856 (vs), 841 (s), 817 (vs), 700 (s), 695 (s), 641 (m), 526 (w), 501 (w) cm^{-1}. Anal. Calcd for $C_6H_2N_3S_3$: C, 33.94; H, 0.95; N, 19.79%. Found: C, 33.80; H, 0.75; N, 19.44%.

Preparation of *S,S′*-Pyrazine-2,3-diyl bis-thioacetate 16. A solution of crude 2,3-pyrazine-(dithiouronium chloride) **15** (1.70 g, 5.64 mmol) prepared by boiling 2,3-dichloropyrazine and thiourea in ethanol,[33] was boiled in 75 mL of water containing 2.0 g of NaOH. The resulting yellow solution was cooled in an ice/water bath and quenched with acetic anhydride to afford a yellow solid which was filtered off, washed with water, and air-dried. Extraction of this solid (1.40 g) with boiling heptane afforded, on cooling, **16** as pale-yellow crystalline flakes, yield 0.75 g (3.3 mmol, 58%), mp 111−113 °C. IR: 1724 (s), 1346 (m), 1170 (w), 1104 (w), 1054 (m), 1004(w), 962 (m), 874 (w), 804 (w), 604 (s) cm^{-1}. ^1H NMR (δ, $CDCl_3$) 8.63 (s, 2H), 2.47 (s, 6H). Anal. Calcd for $C_8H_8N_2S_2O_2$: C, 42.09; H, 3.53; N, 12.27%. Found: C, 41.89; H, 3.65; N, 12.52%.

Preparation of [1,3,2]Pyrazinodithiazolylium Chloride [4][Cl]. The bis-thioacetate **16** (1.14 g, 5.01 mmol) was dissolved in 10 mL of DCE and chlorine gas passed over the solution for 5 min to afford a clear-orange solution. The solvent was flash distilled to leave crude bis(sulfenyl chloride) **17** as a yellow solid. This material was directly redissolved in 10 mL of DCE, and to the stirred solution was added dropwise a solution of trimethylsilyl azide (0.650 g, 5.66 mmol) in 2 mL of DCE, producing a heavy, orange precipitate. After 30 min the product [**4**][Cl] was filtered off, washed with 2 × 15 mL of DCE, and dried in vacuo; yield 0.690 g (3.61 mmol, 72% based on **16**). IR: 3027 (w), 1510 (m), 1341 (w), 1081 (m), 1027 (m), 922 (w), 813 (s), 748 (s), 555(m), 490 (s), 451(w) cm^{-1}.

Preparation of [1,3,2]Pyrazinothiazol-2-yl PDTA 4. Triphenylantimony (0.707 g, 2.00 mmol) was added to a cold (0 °C) slurry of crude [**4**][Cl] (0.690 g, 3.61 mmol) in 7 mL of degassed MeCN and the mixture allowed to warm slowly to room temperature. After 30 min the red/black solid was filtered off, washed with 2 × 10 mL of MeCN, and dried in vacuo. The product **4** was purified by vacuum sublimation at 10^{-2} Torr, yield 0.250 g (1.60 mmol, 44% based on crude [**4**][Cl]), dec 115 °C. Crystals suitable for X-ray work were grown by gradient tube sublimation over a range of 70−30 °C/10^{-2} Torr (sealed tube). IR: 3054 (w), 1525 (m), 1420 (w), 1317 (m), 1219 (w), 1194 (m), 1148 (s), 1168 (m), 850 (m), 694 (s), 688 (s), 503 (w), 482 (m), 432 (s) cm^{-1}. Anal. Calcd for $C_4H_2N_3S$: C, 30.76; H, 1.29; N, 26.90%. Found: C, 31.00; H, 1.18; N, 27.14%.

(33) The procedure follows that described for the analogous quinoxaline compound. See: Morrison, D. C.; Furst, A. *J. Org. Chem.* **1956**, *21*, 470.

EPR Spectra. The X-Band EPR spectra of all the radicals **2**−**8** were recorded at 293 K, using a Bruker EMX-200 spectrometer, on samples dissolved in degassed dichloromethane. Hyperfine coupling constants were obtained by spectral simulation using Simfonia[34] and WinSim. Density functional theory calculations (run on PC workstations using the B3LYP DFT method, as contained in the Gaussian 98W suite of programs, and the 6-31G** basis set) were used to estimate the spin densities and isotropic hyperfine coupling constants.[35] Geometries were optimized within the constraints of C_{2v} symmetry. Full vibrational frequency calculations on the final geometries confirmed that they were stationary points.

Cyclic Voltammetry. Cyclic voltammetry was performed using a PINE Bipotentiostat, model AFCClBP1, with scan rates of 50−100 mV s^{-1} on solutions ($<10^{-3}$ M) of **4**, **8**, and [**6**][SbF_6] in oxygen-free MeCN (dried by distillation from CaH_2) containing 0.1 M tetra-*n*-butylammonium hexafluorophosphate. A sample of salt [**5**][SbF_6] was prepared by metathesis between $NOSbF_6$ and [**5**][Cl] in MeCN, the latter being prepared according to the literature method. Potentials were scanned with respect to the quasi-reference electrode in a single compartment cell fitted with Pt electrodes and referenced to the Fc/Fc^+ couple of ferrocene at 0.38 V vs SCE.[36] The $E_{pa}-E_{pc}$ separation of the reversible couples were within 10% of that of the Fc/Fc^+ couple.

X-ray Measurements. Samples for analysis were glued to a glass fiber with epoxy. X-ray data were collected at 293 and 95 K with a Bruker SMART APEX CCD-based diffractometer using ω-scans of width 0.3° and 30 s duration at a crystal-to-detector distance of 4.908 cm. Intensity decay over the course of the data collections was evaluated by recollecting the first 50 frames of data at the end of the experiment. No significant decay was noted. The reflection data were processed using SAINT.[37] The structures were solved by direct methods using SHELXS-90[38] and refined by least-squares methods on F^2 using SHELXL-97[39] incorporated in the SHELXTL[40] suite of programs. All non-hydrogen atoms were refined anisotropically; hydrogen atoms were located on difference maps and refined isotropically. Details of data collection and refinement are presented in Table 3.

Magnetic Susceptibility Measurements. Magnetic susceptibilities were measured over the temperature range 5−380 K on a George Associates Faraday balance operating at 0.5 T.

Acknowledgment. We thank the Natural Sciences and Engineering Research Council of Canada (NSERCC), the U.S. Office of Basic Energy Sciences, Department of Energy (Grant DE-FG02-97ER45668) and the Office of Naval Research (Contract No. N00014-99-1-0392) for financial support. We also thank the Kentucky Research Challenge Trust Fund for the purchase of CCD X-ray equipment and the upgrade of our X-ray facility, and NSERCC for a post-graduate scholarship to O.P.C.

Supporting Information Available: Details of X-ray crystallographic data collection and structure refinement, tables of atomic coordinates, bond distances and angles, anisotropic thermal parameters, and hydrogen atom positions in CIF format. This information is available free of charge via the Internet at http://pubs.acs.org.

JA048618M

(34) WinEPR Simfonia. Bruker Instruments, Inc., Billerica, MA.
(35) Frisch, M. J.; Trucks, G. W.; Schlegel, H. B.; Scuseria, G. E.; Robb, M. A.; Cheeseman, J. R.; Zakrzewski, V. G.; Montgomery, J. A., Jr.; Stratmann, R. E.; Burant, J. C.; Dapprich, S.; Millam, J. M.; Daniels, A. D.; Kudin, K. N.; Strain, M. C.; Farkas, O.; Tomasi, J.; Barons, V.; Cossi, M.; Cammi, R.; Mennucci, B.; Pomelli, C.; Adamo, C.; Clifford, S.; Ochterski, J.; Petersson, G. A.; Ayala, P. Y.; Cui, Q.; Morokuma, K.; Malick, D. K.; Rabuck, A. D.; Raghavachari, K.; Foreman, J. B.; Cioslowski, J.; Ortiz, J. V.; Stefanov, B. B.; Liu, G.; Fox, D. J.; Keith, T.; Al-Laham, M. A.; Peng, C. Y.; Nanayakkara, A.; Wong, M. W.; Andres, J. L.; Gonzalez, C.; Head-Gordon, M.; Repogle, E. S.; Pople, J. A. *Gaussian 98*, revision A.6; Gaussian, Inc., Pittsburgh, PA, 1998.
(36) Boeré, R. T.; Moock, K. H.; Parvez, M. *Z. Anorg. Allg. Chem.* **1994**, *620*, 1589.
(37) SAINT, version 6.22. Bruker Advanced X-ray Solutions, Inc., Madison, WI. 2001.
(38) Sheldrick, G. M. SHELXS-90. *Acta Crystallogr., Sect. A* **1990**, *46*, 467.
(39) Sheldrick, G. M. SHELXL-97. Program for the Refinement of Crystal Structures, University of Gottingen, Gottingen, Germany, 1997.
(40) SHELXTL, version 6.12. Program Library for Structure Solution and Molecular Graphics, Bruker Advanced X-ray Solutions, Inc., Madison, WI. 2001.